Precambrian Research 349 (2020) 105503

Contents lists available at ScienceDirect

Precambrian Research

journal homepage: www.elsevier.com/locate/precamres

A paired carbonate–organic $\delta^{13}C$ approach to understanding the Cambrian Drumian carbon isotope excursion (DICE)

Dandan Li[a,*], Xiaolin Zhang[a,*], Xu Zhang[a], Hao Zhu[a], Shanchi Peng[b], Lilin Sun[a], Yanan Shen[a]

[a] School of Earth and Space Sciences, University of Science and Technology of China, Hefei 230026, China
[b] Nanjing Institute of Geology and Palaeontology, Chinese Academy of Sciences, Nanjing 210008, China

ARTICLE INFO

Keywords:
Carbon isotope
DICE
Cambrian Series 3
Oceanic anoxia
South China

ABSTRACT

The middle Cambrian (Cambrian Series 3) Drumian carbon isotope excursion (DICE) represents a pronounced negative carbon isotopic excursion, and has been proposed as a key chemostratigraphic marker for identifying the base of Cambrian Drumian Stage and global correlation. However, the precise interbasinal correlation of the DICE to the South China remains unsolved and the driving mechanism of the DICE is to be further understood. In this study, we report new paired $\delta^{13}C_{carb}$ and $\delta^{13}C_{org}$ data from the Wangcun section in South China. Both $\delta^{13}C_{carb}$ and $\delta^{13}C_{org}$ profiles capture a large negative excursion (DICE) near the FAD of *P. atavus*. We suggest that the parallel $\delta^{13}C_{carb}$ and $\delta^{13}C_{org}$ negative excursions during the DICE may have resulted from the shoaling of anoxic deep waters associated with the transgressive event. Shoreward and upward incursion of deep anoxic waters into oxygenated shallower water column during transgression could lead to the enhanced oxidation of dissolved organic carbon (DOC) and introduce additional ^{13}C-depleted carbon to the surface water, resulting in the parallel $\delta^{13}C_{carb}$ and $\delta^{13}C_{org}$ negative excursions. More importantly, we use a box model to quantify the flux of DOC oxidation needed to produce a carbon isotope excursion of the magnitude and duration of the DICE we observed. The model results indicate that oxidation of DOC during the DICE may require massive amounts of oxidants (i.e., sulfate and oxygen), probably causing further expansion of anoxia in the shallow marine environment. We suggest that shoaling of anoxic water during the DICE could have delayed the recovery of metazoan reef systems from the early–middle Cambrian mass extinctions.

1. Introduction

A series of mass extinctions occurred during the early–middle Cambrian transition, resulting in the demise of the Archaeocyathids and severe generic-level losses of olenellid and redlichiid trilobites (Zhuravlev and Wood, 1996; Palmer, 1998; Li et al., 2007; Peng et al., 2012; Adachi et al., 2014). The longest post extinction metazoan "reef gap" in the Phanerozoic was documented following these early–middle Cambrian events (Boucot, 1990; Wood, 1999; Adachi et al., 2014). The middle Cambrian (Cambrian Series 3) thus represents a key post-extinction interval. The interval leading up to the worldwide absence of metazoan reef systems in the middle Cambrian was a time of extreme paleoenvironmental oscillations, including carbon isotope excursions (e.g., Babcock et al., 2007; Ahlberg et al., 2009; Peng et al., 2009), eruptions of large igneous provinces (LIPs) (Glass and Phillips, 2006; Jourdan et al., 2014), sea-level changes (e.g., Babcock et al., 2007; Peng et al., 2009; Elfar et al., 2017), and widespread marine anoxia (e.g., Howley and Jiang, 2010; Pagès and Schmid, 2016; Pagès et al., 2016). Associated middle Cambrian carbonates in South China, Scotland, Scania, Great Basin (USA), Georgina Basin (Australia), among others, revealed an abrupt and prominent decrease in $\delta^{13}C$, referred to as DICE (Babcock et al., 2007; Ahlberg et al., 2009; Howley and Jiang, 2010; Lehnert et al., 2013; Pagès and Schmid, 2016; Faggetter et al., 2016). The DICE event is considered evidence of a profound disturbance to the global carbon cycle, and may have resulted from chemical changes in the ocean-atmosphere system (Kump and Arthur, 1999; Howley and Jiang, 2010; Pagès and Schmid, 2016). If this interpretation is correct, the DICE event can then be used to probe potential linkages between chemical conditions in the ocean-atmosphere system and metazoan evolution during the middle Cambrian.

The globally recognized middle Cambrian DICE is characterized by a 2‰ to 4‰ negative shift in carbon isotopic composition of carbonates ($\delta^{13}C_{carb}$) that coincides with the FAD of agnostoid arthropod *Ptychagnostus atavus* at the beginning of the Cambrian Series 3 Drumian Stage, about 506.5 million years ago (e.g., Babcock et al., 2007; Howley and Jiang, 2010; Peng et al., 2012). The DICE corresponds closely with

* Corresponding authors.
E-mail addresses: danshine@ustc.edu.cn (D. Li), zhxl2012@ustc.edu.cn (X. Zhang).

https://doi.org/10.1016/j.precamres.2019.105503
Received 26 March 2019; Received in revised form 16 July 2019; Accepted 11 October 2019
Available online 21 October 2019

the shift in the biofacies of the agnostoid trilobite assemblages (e.g., Peng and Robison, 2000; Babcock et al., 2007), and it is suggested to have been associated with a transgressive event in Laurentia, South China, Scotland, and Baltica (Babcock et al., 2007; Ahlberg et al., 2009; Peng et al., 2009; Faggetter et al., 2016; Elfar et al., 2017).

For this study, we target the Wangcun section in South China which contains continuous strata from the Wuliuan Stage to the Guzhangian Stage (Peng et al., 2009). The middle Cambrian successions from the Yangtze platform, South China are critical stratigraphic units that serve as a window for understanding the environmental significance of the DICE and its potential link to biological events. Preliminary carbon isotopic data from the middle Cambrian in South China have been presented (Zhu et al., 2004; Peng et al., 2009). However, the DICE has not been well documented. Here we present high-resolution paired carbon isotopic analyses of carbonates ($\delta^{13}C_{carb}$) and organic carbon ($\delta^{13}C_{org}$) for the Wangcun section, which provide a high-resolution carbon isotope stratigraphic framework for the middle Cambrian in South China. Furthermore, the DICE identified in the Wangcun section can be used for interbasinal correlation and to improve our understanding of the middle Cambrian ocean chemistry.

2. Geological setting

The Wangcun section is exposed along a road cut on the north bank of the Yongshui River in the Wuling Mountains, Hunan Province (109°58′ E, 28°43′ N; Fig. 1) (Peng et al., 2009). It appears to be a parastratotype section of the Luoyixi section (GSSP for the base of the Guzhangian Stage), which is just across the Yongshui River. The Wangcun section was deposited in the lower part of an outer slope-apron environment (Pu and Ye, 1991; Peng and Babcock, 2001; Peng et al., 2009). The Cambrian strata of the Wangcun section is subdivided into the Aoxi and Huaqiao formations in ascending order (Fig. 2). The Aoxi Formation is mainly composed of dolostone and black shale interbedded with limestone, while the Huaqiao Formation mostly consists of fine-grained carbonate (Peng et al., 2009) (Fig. 2). The Wangcun section and its trilobite-rich succession have been well documented in terms of lithology and biostratigraphy (Peng and Robison, 2000; Peng et al., 2009). Zonally diagnostic trilobites identified at the Wangcun section include, in ascending order: *P. gibbus* Zone, *P. atavus* Zone, *P. punctuosus* Zone, *G. nathorsti* Zone, *L. atmata* Zone, *L. laevigata* Zone, and *P. bulbus* Zone (Fig. 2).

3. Analytical methods

For $\delta^{13}C_{carb}$ analysis, approximately 150 μg of sample powder was reacted with 3–5 drops of ~103% phosphoric acid at 70 °C in a Kiel IV carbonate device attached to a Thermo Finnigan MAT 253 mass-spectrometer at University of Science and Technology of China. Isotope ratios are reported in per mil relative to the Vienna Pee Dee Belemnite (V-PDB) standard. Precision and calibration of data were monitored through routine analysis of a domestic carbonate standard (GBW04416) and internal laboratory standards. Analytical uncertainties on $\delta^{13}C_{carb}$

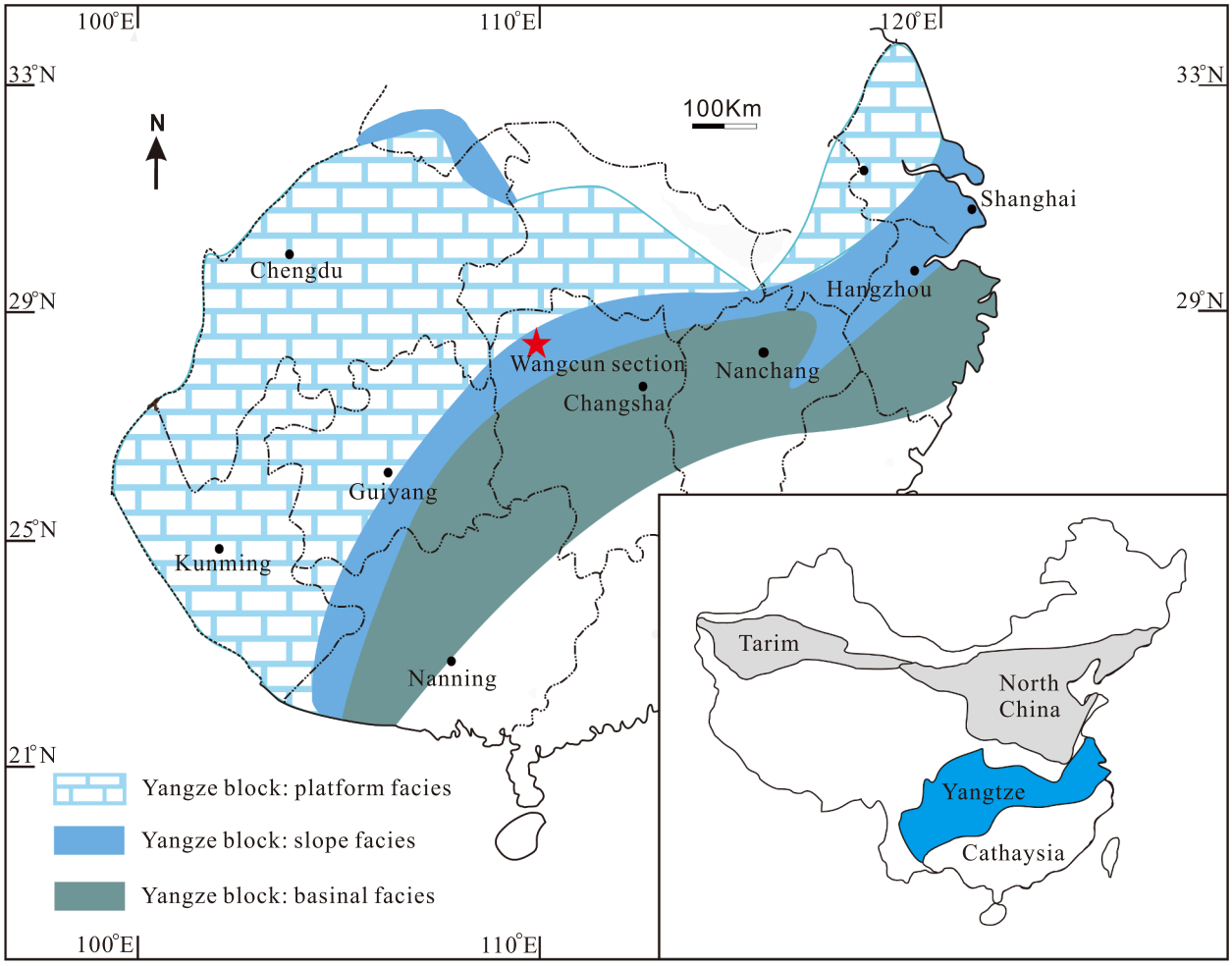

Fig. 1. A generalized paleogeographic reconstruction for the Yangtze Craton (modified after Pu and Ye, 1991; Peng and Babcock, 2001). The location of Wangcun section is marked by a red star. The inset is a geological map of China with the location of the Yangtze Craton of South China highlighted in blue. (For interpretation of the references to colour in this figure legend, the reader is referred to the web version of this article.)

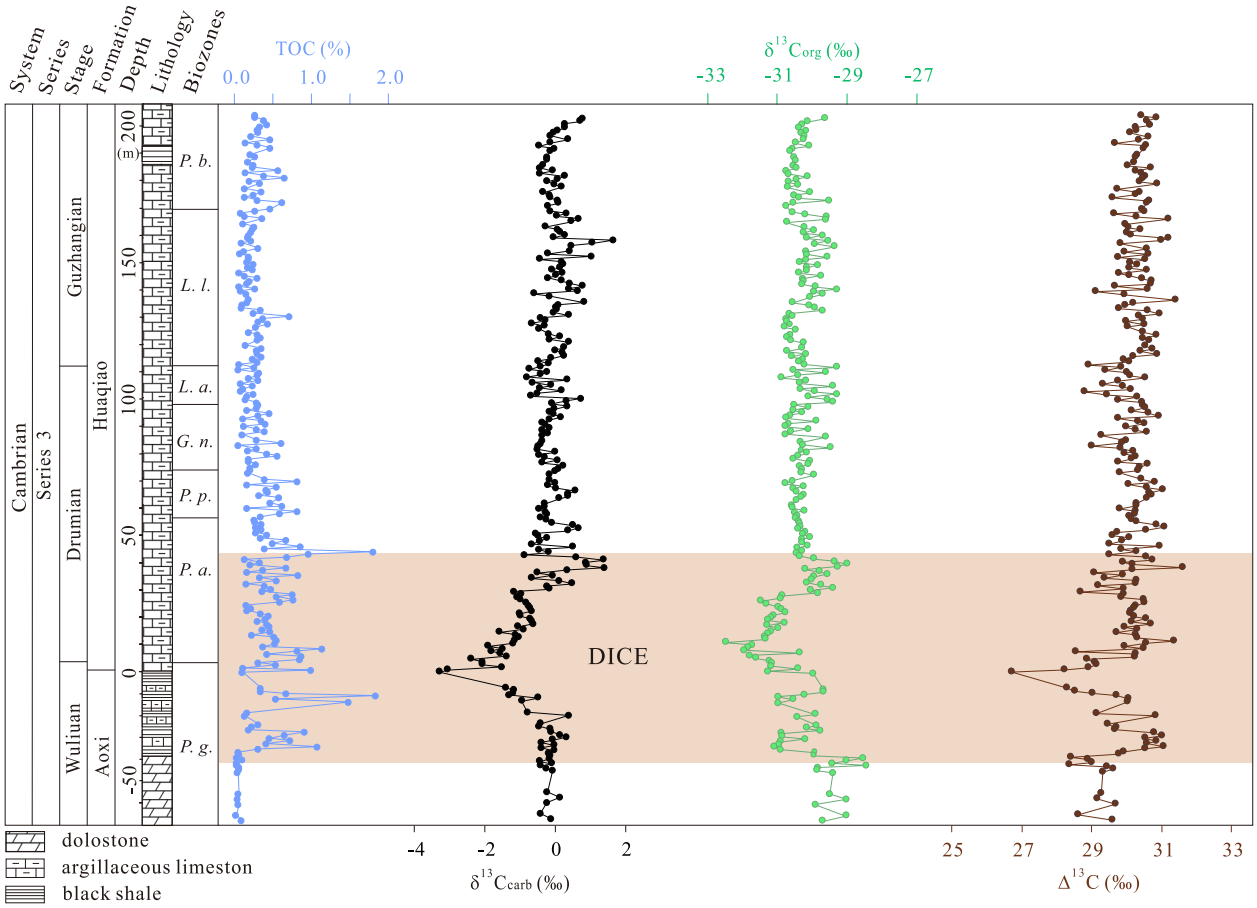

Fig. 2. The TOC, $\delta^{13}C_{carb}$, $\delta^{13}C_{org}$, and $\Delta^{13}C$ profiles across the Wuliuan Stage to the Guzhangian Stage from the Wangcun section. Trilobite zones: *P.b.* – *P. bulbus* Zone; *L.l.* – *L. laevigata* Zone; *L.a.* – *L. atmata* Zone; *G.n.* – *G. nathorsti* Zone; *P.p.* – *P. punctuosus* Zone; *P.a.* – *P. atavus* Zone; *P.g.* – *P. gibbus* Zone.

and $\delta^{18}O$ analyses are better than 0.05‰ and 0.06‰, respectively (one sigma).

For $\delta^{13}C_{org}$ analysis, sample powder was first treated repeatedly with 6 N HCl to remove carbonates and other acid-soluble minerals. The residual powder was then rinsed several times with Milli-Q water and dried in an oven at 70 °C. $\delta^{13}C_{org}$ and total organic carbon (TOC) were analyzed at the University of Science and Technology of China using an Elemental Analyzer attached to a Thermo Finnigan MAT 253 mass-spectrometer configured in continuous flow mode. Isotope ratios are reported in delta notation as per mil (‰) relative to the V-PDB standard. Precision and calibration of data were monitored through routine analysis of an internal laboratory and the international standard IAEA-600 (caffeine). Standard deviation for $\delta^{13}C_{org}$ is less than 0.1‰ (one sigma).

4. Results

The TOC content, $\delta^{13}C_{carb}$ and $\delta^{13}C_{org}$ of 226 samples were analyzed, spanning a stratigraphic interval of 261.5 m from the Wangcun section (Fig. 2, Table 1). The TOC content ranges from 0.02% to 1.84%. The highest TOC values and also the most variability in TOC concentrations occur near the base of the section (Fig. 2). TOC concentration and variability decreases toward the top of the section.

A strong negative $\delta^{13}C_{carb}$ shift from ~0‰ down to −3.3‰ and a roughly contemporaneous negative $\delta^{13}C_{org}$ shift from ~−29‰ to a minimum of −32.5‰ are observed near the boundary between the Wuliuan Stage and the Drumian Stage (i.e., DICE, Fig. 2). Carbon isotopic values return to normal approximately 40 m above the Wuliuan–Drumian boundary. From the *P. punctuosus* Zone to *P. bulbus* Zone, the $\delta^{13}C_{carb}$ and $\delta^{13}C_{org}$ values are relatively stable around 0‰ and −30‰, respectively (Fig. 2). The difference between the $\delta^{13}C_{carb}$ and $\delta^{13}C_{org}$ (i.e., $\Delta^{13}C$) records a negative trend with the lowest values (~26.7‰) near the boundary of the Aoxi and Huaqiao formations, slightly before the Wuliuan–Drumian boundary (Fig. 2). Higher in the section, $\Delta^{13}C$ values above +7.6 m are maintained at around 30‰ (Fig. 2).

5. Discussion

5.1. Data evaluation

It has been suggested that the carbon isotopic composition of sedimentary carbonate and organic matters can be altered by post-depositional processes (Irwin et al., 1977; Allan and Matthews, 1982; Kaufman and Knoll, 1995; Derry, 2010). Therefore, it is essential to evaluate the reliability of our isotope data prior to the use of carbon isotopes in stratigraphic correlation and paleoenvironmental reconstruction.

Carbonate is susceptible to isotopic exchange with meteoric waters and pore fluids in marine sediments during early diagenesis (Irwin et al., 1977; Allan and Matthews, 1982). Progressive diagenetic alteration can lower $\delta^{13}C$ and $\delta^{18}O$ values in marine carbonates, resulting in co-variations between the $\delta^{13}C_{carb}$ and $\delta^{18}O$ (Allan and Matthews, 1982). Consequently, samples with $\delta^{18}O < -10‰$ and $\delta^{13}C_{carb}$ values that positively correlated with $\delta^{18}O$ are often thought of as having been affected by diagenesis (Kaufman and Knoll, 1995). In the present case, most of $\delta^{18}O$ values are heavier than −10‰, except for a few samples in the upper part of the DICE and the Guzhangian Stage (Table 1). In addition, our data display little correlation between $\delta^{13}C_{carb}$ and $\delta^{18}O$ for the entire dataset ($R^2 = 0.08$) and across DICE event ($R^2 = 0.00$)

Table 1
$\delta^{13}C_{carb}$, $\delta^{18}O$, $\delta^{13}C_{org}$, $\Delta^{13}C$ and TOC of samples from the Wangcun section, Hunan, SW China.

Sample	Depth (m)	$\delta^{13}C_{carb}$ (‰)	$\delta^{18}O$ (‰)	$\delta^{13}C_{org}$ (‰)	$\Delta^{13}C$ (‰)	TOC (%)
LYX 203.5	203.5	0.79	−9.23	−29.65	30.43	0.27
LYX 202.5	202.5	0.72	−9.02	−30.14	30.86	0.27
LYX 201.5	201.5	0.29	−9.35	−30.31	30.59	0.38
LYX 200	200	0.29	−8.80	−30.39	30.68	0.43
LYX 199	199	0.08	−8.75	−30.19	30.27	0.33
LYX 198	198	−0.04	−9.03	−30.33	30.30	0.30
LYX 197	197	−0.13	−10.20	−30.22	30.09	0.31
LYX 195.7	195.7	0.37	−9.87	−30.26	30.63	0.22
LYX 194.5	194.5	−0.12	−9.22	−30.47	30.35	0.47
LYX 193.3	193.3	−0.44	−11.68	−30.10	29.66	0.15
LYX 192.3	192.3	−0.01	−10.09	−30.57	30.56	0.30
LYX 191.3	191.3	−0.14	−8.51	−30.63	30.50	0.46
LYX 189	189	−0.23	−9.98	−30.52	30.30	0.21
LYX 188	188	−0.22	−9.60	−30.48	30.26	0.27
LYX 186	186	−0.34	−9.69	−30.55	30.21	0.18
LYX 185	185	−0.42	−9.14	−30.45	30.03	0.25
LYX 184	184	−0.07	−9.59	−30.76	30.69	0.24
LYX 183	183	−0.42	−8.58	−30.68	30.27	0.57
LYX 182	182	0.28	−9.19	−30.14	30.43	0.15
LYX 181	181	0.08	−8.62	−30.46	30.54	0.39
LYX 180	180	−0.21	−8.95	−30.69	30.48	0.66
LYX 179	179	−0.02	−9.10	−30.40	30.38	0.20
LYX 178	178	0.19	−8.41	−30.70	30.89	0.33
LYX 176	176	−0.33	−8.98	−30.07	29.73	0.14
LYX 175	175	−0.16	−8.37	−30.53	30.37	0.36
LYX 174	174	−0.14	−7.87	−30.39	30.26	0.25
LYX 173	173	0.09	−9.25	−29.52	29.61	0.14
LYX 172	172	0.10	−8.45	−30.56	30.66	0.30
LYX 171	171	−0.19	−8.94	−30.76	30.57	0.62
LYX 168.8	168.8	−0.14	−9.26	−30.58	30.44	0.47
LYX 168	168	0.32	−8.72	−30.20	30.52	0.27
LYX 167	167	0.06	−9.30	−29.59	29.64	0.08
LYX 166	166	0.68	−9.26	−29.61	30.29	0.14
LYX 165	165	0.48	−9.69	−30.73	31.21	0.36
LYX 163	163	−0.27	−9.22	−30.23	29.96	0.11
LYX 162	162	0.09	−8.33	−29.97	30.05	0.26
LYX 161	161	0.14	−9.19	−30.25	30.39	0.24
LYX 160	160	0.30	−11.09	−29.71	30.01	0.22
LYX 159	159	−0.04	−9.40	−30.17	30.13	0.19
LYX 158	158	1.66	−9.42	−29.54	31.20	0.17
LYX 157	157	1.07	−8.94	−29.93	30.99	0.22
LYX 156	156	0.47	−9.22	−29.36	29.83	0.10
LYX 154	154	0.42	−8.70	−30.18	30.59	0.32
LYX 153	153	−0.20	−9.16	−30.15	29.95	0.13
LYX 152	152	1.05	−8.62	−29.58	30.63	0.08
LYX 151	151	−0.43	−8.43	−30.19	29.76	0.19
LYX 150	150	0.18	−9.10	−30.36	30.54	0.19
LYX 149	149	0.24	−9.42	−29.85	30.10	0.17
LYX 148	148	0.15	−9.25	−30.15	30.30	0.25
LYX 147	147	−0.09	−8.77	−30.16	30.07	0.18
LYX 146	146	0.21	−9.32	−30.38	30.59	0.23
LYX 145	145	0.04	−9.00	−29.75	29.79	0.06
LYX 144	144	−0.19	−9.40	−30.27	30.09	0.13
LYX 143	143	0.19	−9.21	−30.26	30.45	0.31
LYX 142	142	0.42	−7.61	−30.30	30.72	0.20
LYX 141	141	0.79	−9.42	−29.91	30.70	0.16
LYX 140	140	0.39	−10.05	−29.29	29.68	0.07
LYX 139.1	139.1	0.66	−9.12	−29.95	30.61	0.28
LYX 138.1	138.1	−0.60	−9.37	−29.71	29.12	0.08
LYX 137.1	137.1	−0.14	−9.42	−30.08	29.94	0.16
LYX 135	135	0.82	−9.12	−30.57	31.40	0.19
LYX 134	134	0.10	−9.05	−30.09	30.19	0.17
LYX 133	133	0.04	−9.47	−29.93	29.97	0.10
LYX 132	132	0.07	−9.42	−29.72	29.78	0.09
LYX 131	131	−0.05	−9.10	−30.65	30.61	0.35
LYX 130	130	0.39	−9.52	−30.57	30.96	0.25
LYX 129	129	−0.40	−8.86	−30.75	30.35	0.72
LYX 128	128	−0.26	−7.83	−30.74	30.48	0.37
LYX 127	127	−0.66	−8.27	−30.64	29.98	0.31
LYX 126	126	−0.30	−9.00	−30.81	30.51	0.44
LYX 125	125	−0.45	−9.07	−30.48	30.03	0.29
LYX 123	123	−0.17	−9.66	−30.64	30.46	0.19
LYX 122	122	0.14	−9.79	−30.72	30.86	0.31
LYX 121	121	−0.16	−9.83	−30.63	30.47	0.35

(*continued on next page*)

Table 1 (*continued*)

Sample	Depth (m)	$\delta^{13}C_{carb}$ (‰)	$\delta^{18}O$ (‰)	$\delta^{13}C_{org}$ (‰)	$\Delta^{13}C$ (‰)	TOC (%)
LYX 120	120	0.40	−8.85	−30.24	30.64	0.30
LYX 118	118	0.26	−9.68	−30.29	30.55	0.15
LYX 117	117	0.00	−8.39	−30.74	30.74	0.35
LYX 116	116	0.22	−8.54	−30.19	30.41	0.29
LYX 115	115	0.27	−9.52	−30.61	30.87	0.30
LYX 114	114	−0.09	−8.59	−30.29	30.19	0.36
LYX 113	113	−0.47	−8.21	−30.39	29.92	0.24
LYX 112	112	−0.16	−8.94	−30.24	30.08	0.31
LYX 111	111	−0.39	−9.54	−29.30	28.91	0.07
LYX 110	110	−0.72	−8.11	−30.56	29.84	0.26
LYX 109	109	−0.22	−9.73	−29.61	29.39	0.06
LYX 108	108	−0.40	−8.34	−30.41	30.01	0.32
LYX 107	107	−0.79	−8.52	−30.90	30.11	0.30
LYX 106	106	0.36	−9.53	−30.18	30.54	0.19
LYX 105	105	−0.62	−9.00	−30.37	29.75	0.31
LYX 104	104	−0.09	−9.75	−29.41	29.32	0.08
LYX 103	103	−0.44	−8.57	−30.34	29.90	0.24
LYX 102	102	0.20	−9.65	−29.94	30.13	0.11
LYX 101	101	−0.49	−9.61	−29.29	28.80	0.08
LYX 100	100	−0.67	−8.70	−30.11	29.44	0.26
LYX 99	99	0.74	−9.81	−29.58	30.31	0.16
LYX 98	98	0.34	−9.57	−29.42	29.76	0.14
LYX 97	97	−0.09	−7.90	−30.54	30.45	0.29
LYX 96	96	0.36	−9.24	−30.11	30.47	0.31
LYX 95	95	−0.01	−9.50	−30.54	30.54	0.29
LYX 94	94	−0.15	−9.58	−30.30	30.15	0.16
LYX 93	93	−0.03	−8.91	−30.65	30.62	0.46
LYX 92	92	0.17	−8.28	−30.75	30.92	0.32
LYX 91	91	−0.15	−9.45	−29.90	29.75	0.11
LYX 90	90	−0.37	−9.17	−30.69	30.33	0.35
LYX 89	89	−0.26	−9.15	−30.78	30.52	0.41
LYX 88	88	−0.14	−9.73	−30.12	29.98	0.12
LYX 87	87	−0.36	−8.39	−30.62	30.27	0.30
LYX 86	86	−0.19	−9.44	−30.77	30.58	0.39
LYX 85	85	−0.35	−9.69	−29.62	29.27	0.11
LYX 83	83	−0.35	−8.40	−30.34	29.98	0.30
LYX 82	82	−0.40	−8.27	−30.27	29.86	0.62
LYX 81	81	−0.48	−9.93	−29.49	29.01	0.05
LYX 80	80	−0.50	−7.95	−30.33	29.82	0.29
LYX 79	79	0.01	−9.66	−30.17	30.18	0.18
LYX 78	78	−0.45	−7.51	−30.40	29.95	0.43
LYX 77	77	−0.29	−7.57	−30.54	30.26	0.56
LYX 76	76	0.09	−8.76	−30.06	30.15	0.19
LYX 75	75	−0.35	−9.70	−30.11	29.76	0.19
LYX 74	74	0.24	−9.74	−30.36	30.60	0.28
LYX 72.8	72.8	0.09	−9.34	−30.29	30.38	0.21
LYX 71.8	71.8	0.01	−9.48	−30.32	30.32	0.20
LYX 70.8	70.8	−0.15	−9.90	−29.96	29.81	0.17
LYX 68.6	68.6	−0.16	−7.38	−30.58	30.42	0.39
LYX 67.6	67.6	0.02	−7.14	−30.79	30.81	0.82
LYX 66.6	66.6	−0.20	−9.49	−30.26	30.06	0.17
LYX 65.6	65.6	0.03	−7.55	−30.55	30.58	0.56
LYX 64.6	64.6	0.59	−9.75	−30.46	31.04	0.41
LYX 63.6	63.6	0.39	−9.61	−30.26	30.65	0.43
LYX 62.6	62.6	0.39	−9.83	−30.33	30.72	0.33
LYX 61.6	61.6	0.14	−8.40	−30.46	30.59	0.58
LYX 59.6	59.6	−0.30	−9.12	−30.59	30.30	0.46
LYX 58.6	58.6	−0.29	−8.28	−30.57	30.28	0.62
LYX 57.6	57.6	−0.44	−8.49	−30.24	29.80	0.17
LYX 56.6	56.6	−0.26	−8.78	−30.51	30.26	0.82
LYX 55.6	55.6	−0.21	−9.54	−30.44	30.23	0.60
LYX 54.6	54.6	−0.40	−8.59	−30.49	30.09	0.35
LYX 53.6	53.6	−0.25	−9.09	−30.39	30.15	0.26
LYX 52.7	52.7	−0.08	−9.49	−30.36	30.28	0.27
LYX 51.7	51.7	0.52	−7.86	−30.35	30.87	0.35
LYX 50.7	50.7	0.66	−9.77	−30.42	31.09	0.28
LYX 49.7	49.7	0.37	−9.57	−30.20	30.57	0.36
LYX 48.7	48.7	−0.54	−9.92	−30.27	29.73	0.28
LYX 47.7	47.7	−0.47	−7.72	−30.08	29.60	0.42
LYX 46.8	46.8	−0.23	−9.88	−30.30	30.07	0.34
LYX 45.8	45.8	−0.42	−8.64	−30.29	29.87	0.68
LYX 44.6	44.6	−0.64	−7.40	−30.14	29.50	0.50
LYX 43.6	43.6	0.52	−7.78	−30.43	30.95	0.87
LYX 42.6	42.6	−0.45	−9.32	−30.30	29.85	0.39
LYX 41.6	41.6	−0.17	−7.91	−30.45	30.28	1.81

(*continued on next page*)

Table 1 (*continued*)

Sample	Depth (m)	$\delta^{13}C_{carb}$ (‰)	$\delta^{18}O$ (‰)	$\delta^{13}C_{org}$ (‰)	$\Delta^{13}C$ (‰)	TOC (%)
LYX 40.6	40.6	−0.85	−7.60	−30.36	29.51	0.97
LYX 39.7	39.7	0.61	−8.79	−29.97	30.57	0.68
LYX 38.7	38.7	1.39	−9.97	−29.36	30.75	0.14
LYX 37.7	37.7	0.89	−9.59	−29.01	29.90	0.33
LYX 36.8	36.8	0.89	−9.83	−29.28	30.18	0.21
LYX 35.8	35.8	1.40	−9.17	−30.22	31.61	0.68
LYX 34.9	34.9	0.36	−11.10	−29.80	30.16	0.38
LYX 33.9	33.9	−0.49	−10.61	−29.56	29.07	0.17
LYX 32.9	32.9	−0.07	−6.85	−29.95	29.89	0.83
LYX 31.9	31.9	−0.66	−8.79	−30.03	29.37	0.33
LYX 30.9	30.9	0.13	−9.17	−30.17	30.29	0.55
LYX 29.9	29.9	0.50	−9.83	−29.76	30.26	0.15
LYX 28.9	28.9	−0.22	−9.05	−29.41	29.19	0.39
LYX 27.9	27.9	−0.15	−9.04	−30.06	29.91	0.48
LYX 26.9	26.9	−1.16	−9.93	−29.84	28.68	0.37
LYX 25.9	25.9	−0.96	−6.43	−30.87	29.91	0.76
LYX 24.9	24.9	−1.07	−6.12	−30.92	29.85	0.55
LYX 23.9	23.9	−0.98	−6.24	−31.47	30.49	0.77
LYX 22.9	22.9	−0.81	−6.37	−31.33	30.52	0.59
LYX 21.7	21.7	−0.74	−9.80	−30.99	30.25	0.16
LYX 20.7	20.7	−0.69	−5.51	−30.90	30.21	0.22
LYX 19.7	19.7	−0.65	−5.60	−30.78	30.14	0.16
LYX 18.7	18.7	−1.00	−5.74	−31.11	30.11	0.34
LYX 17.8	17.8	−0.98	−5.72	−31.19	30.21	0.45
LYX 16.8	16.8	−0.70	−6.10	−31.27	30.57	0.41
LYX 15.8	15.8	−0.65	−5.85	−30.81	30.16	0.30
LYX 14.8	14.8	−0.62	−5.52	−31.30	30.69	0.42
LYX 13.8	13.8	−1.05	−6.57	−30.99	29.94	0.45
LYX 12.8	12.8	−0.87	−9.66	−31.18	30.31	0.36
LYX 11.8	11.8	−1.56	−5.52	−31.27	29.71	0.47
LYX 10.8	10.8	−1.11	−10.38	−31.37	30.26	0.23
LYX 9.8	9.8	−1.03	−6.68	−31.34	30.31	0.52
LYX 8.6	8.6	−1.13	−10.18	−32.49	31.36	0.55
LYX 7.6	7.6	−1.18	−8.11	−31.74	30.56	0.53
LYX 6.6	6.6	−1.89	−9.70	−31.84	29.95	0.38
LYX 5.6	5.6	−1.47	−6.19	−31.97	30.50	1.15
LYX 4.7	4.7	−1.81	−6.22	−30.36	28.55	0.82
LYX 3.7	3.7	−1.54	−10.44	−31.81	30.27	0.43
LYX 2.7	2.7	−1.37	−6.99	−31.61	30.24	0.87
LYX 1.7	1.7	−2.37	−6.17	−31.23	28.86	0.86
LYX 0.7	0.7	−2.06	−10.03	−31.16	29.09	0.31
LYX-0.3	−0.3	−2.06	−10.33	−31.20	29.14	0.54
LYX-1.3	−1.3	−1.50	−10.90	−30.41	28.92	0.12
LYX-2.3	−2.3	−3.05	−9.31	−31.27	28.23	1.00
LYX-3.0	−3	−3.26	−10.54	−29.98	26.72	0.10
LYX-9.0	−9	−1.40	−7.56	−29.68	28.29	0.35
LYX-10	−10	−1.16	−3.75	−29.69	28.53	0.35
LYX-11	−11	−1.19	−3.44	−30.23	29.04	0.67
LYX-11.8	−11.8	−1.29	−4.11	−30.99	29.71	1.84
LYX-12.8	−12.8	−0.48	−4.60	−30.54	30.06	0.54
LYX-14	−14	−0.94	−4.50	−30.97	30.04	1.48
LYX-18.2	−18.2	−0.77	−4.79	−29.91	29.14	0.17
LYX-19.3	−19.3	0.40	−7.31	−30.44	30.84	0.14
LYX-22.3	−22.3	−0.41	−5.08	−29.88	29.47	0.31
LYX-23.3	−23.3	−0.45	−5.50	−30.17	29.72	0.23
LYX-24.3	−24.3	−0.12	−5.07	−29.78	29.66	0.19
LYX-25.3	−25.3	−0.10	−5.24	−30.89	30.79	0.91
LYX-26.5	−26.5	0.14	−5.42	−30.87	31.01	0.65
LYX-27.5	−27.5	0.34	−5.00	−30.20	30.54	0.45
LYX-28.5	−28.5	−0.06	−6.43	−30.91	30.85	0.72
LYX-29.5	−29.5	−0.39	−7.23	−30.96	30.57	0.42
LYX-30.5	−30.5	−0.02	−5.86	−31.09	31.07	1.09
LYX-31.5	−31.5	−0.39	−6.30	−30.93	30.54	0.32
LYX-32.5	−32.5	−0.01	−9.01	−29.92	29.91	0.05
LYX-33.5	−33.5	−0.16	−8.68	−29.95	29.79	0.07
LYX-34.5	−34.5	−0.14	−8.97	−28.54	28.41	0.03
LYX-35.5	−35.5	−0.14	−8.92	−29.03	28.89	0.10
LYX-36.5	−36.5	−0.42	−9.01	−29.42	29.00	0.04
LYX-37.3	−37.3	−0.09	−8.41	−28.45	28.36	0.03
LYX-38.1	−38.1	−0.40	−8.33	−29.84	29.44	0.06
LYX-39.1	−39.1	−0.25	−7.88	−29.87	29.63	0.06
LYX-40	−40	−0.07	−8.95	−29.40	29.33	0.04
LYX-48	−48	−0.22	−8.97	−29.49	29.27	0.05
LYX-50	−50	0.15	−8.70	−29.02	29.17	0.04
LYX-52	−52	−0.22	−8.82	−29.91	29.69	0.05

(*continued on next page*)

Table 1 (*continued*)

Sample	Depth (m)	$\delta^{13}C_{carb}$ (‰)	$\delta^{18}O$ (‰)	$\delta^{13}C_{org}$ (‰)	$\Delta^{13}C$ (‰)	TOC (%)
LYX-56	−56	−0.41	−8.91	−29.03	28.61	0.02
LYX-58	−58	−0.10	−8.96	−29.70	29.60	0.10

(Fig. 3A), which exclude the possibility of post-depositional fluid alteration. Moreover, even carbonate samples with extremely low $\delta^{18}O$ values (< −10‰) may have preserved primary carbon isotope signatures, as has been widely reported in recent studies of Cambrian carbonate strata worldwide (Li et al., 2013; Ishikawa et al., 2014; Li et al., 2017). This can be attributed to the differing susceptibility of oxygen and carbon isotopes to diagenetic alteration during early diagenesis. It is generally accepted that the carbon isotopic composition is less susceptible to diagenetic alteration and thus reflects primary changes in the carbon cycle (Banner and Hanson, 1990; Gao and Land, 1991; Derry, 2010). This is because diagenetic fluids have typically low carbon contents compared to carbonate rocks (Derry et al., 1994; Kaufman and Knoll, 1995), and significant alteration of the primary $\delta^{13}C$ values during meteoric diagenesis requires high water/rock ratios of ≥1000, which is almost impossible under realistic conditions (Banner and Hanson, 1990; Gao and Land, 1991). In contrast, the oxygen isotopic composition of carbonate rocks is more sensitive to post-depositional diagenesis given the high oxygen content and potentially very different $\delta^{18}O$ values of the diagenetic fluid (e.g., Kaufman and Knoll, 1995). We therefore suggest that near primary $\delta^{13}C_{carb}$ signatures have been effectively preserved in the samples collected from the Wangcun section.

The $\delta^{13}C_{org}$ values in sedimentary rocks can be altered by degradation during post depositional processes (Hayes et al., 1983; Schidlowski and Aharon, 1992). With increased organic matter degradation during diagenesis/thermal maturation, ^{12}C is kinetically preferentially removed (Hayes et al., 1983; Schidlowski and Aharon, 1992). Consequently, organic matter that are ^{13}C-enriched are expected to have lower TOC. There is, however, no statistically significant correlation between TOC and $\delta^{13}C_{org}$ for the entire dataset ($R^2 = 0.28$) and across DICE event ($R^2 = 0.17$) (Fig. 3B), despite the wide range of TOC. This suggests that there is little significant diagenetic alteration of the Wangcun $\delta^{13}C_{org}$ record.

The geochemical tests discussed above argue against substantial diagenetic alteration of $\delta^{13}C_{carb}$ and $\delta^{13}C_{org}$ values of the Wangcun section. In addition, our isotopic data show that $\delta^{13}C_{carb}$ and $\delta^{13}C_{org}$ values began to decrease within the interbeded black shale and limestone at the top of the Aoxi Formation (Fig. 2), and reach their lowest values near the lithological transition from black shale to thickly bedded limestone (i.e., the contact between the Aoxi and Huaqiao formations), and then increase to pre-event values in the limestones (Fig. 2). No apparent relationship between $\delta^{13}C$ variations and lithological changes implies that the carbon isotope signatures are not controlled primarily by depositional environments and/or geological setting. Therefore, it is reasonable to conclude that the $\delta^{13}C_{carb}$ and $\delta^{13}C_{org}$ of the Wangcun section reflect variation in the isotopic composition of contemporaneous seawater, and that the $\delta^{13}C$ data can be used for stratigraphic correlation and paleoenvironmental reconstruction.

5.2. Global correlation of the DICE to the $\delta^{13}C$ profile from South China

The DICE has been observed from stratigraphic units worldwide and can be well correlated using chemo- and biostratigraphic data (Álvaro et al., 2008; Ahlberg et al., 2009; Howley and Jiang, 2010; Lehnert et al., 2013; Pagès and Schmid, 2016). Globally, the DICE is coincident with the base of the Drumian Stage (e.g., Babcock et al. 2007; Howley and Jiang, 2010; Peng et al., 2012). However, the data from a previous study shows that the $\delta^{13}C_{carb}$ profile of the Wangcun section in South China contains a large negative excursion below the FAD of *P. atavus* and a small negative excursion above the base of Drumian Stage (Zhu et al., 2004), leading to a questionable global correlation of DICE from South China (Howley and Jiang, 2010; Pagès and Schmid, 2016). Intriguingly, there is only one large $\delta^{13}C_{carb}$ negative excursion recorded near the FAD of *P. atavus* in our study rather than two negative excursions reported by Zhu et al. (2004). The inconsistent expression of the DICE in the Wangcun section between our study and Zhu et al. (2004) may be due to the higher sampling resolution in this study (i.e., 1 m versus 10 m). Hence, the negative $\delta^{13}C$ excursion near the FAD of *P. atavus* observed in our study provides an opportunity for the accurate correlation of the DICE from South China to the global carbon isotope curve.

Fig. 4 shows the correlation of the DICE between our study and other sedimentary basins worldwide. The $\delta^{13}C_{carb}$ profiles include the isotopic data from the Wangcun section in South China, a composite stratigraphic section constructed from five sections in the Great Basin

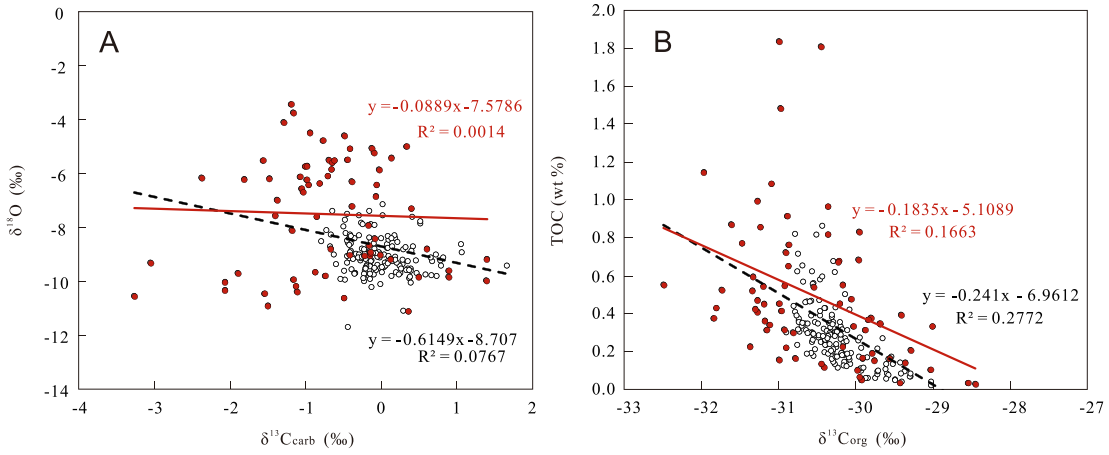

Fig. 3. Cross-plots of $\delta^{13}C_{carb}$ and $\delta^{18}O$ (A), and $\delta^{13}C_{org}$ and TOC (B) for the Wangcun section. The solid red circles indicate samples from the DICE. The solid red circles and the open black circles together represent samples from the entire dataset. (For interpretation of the references to colour in this figure legend, the reader is referred to the web version of this article.)

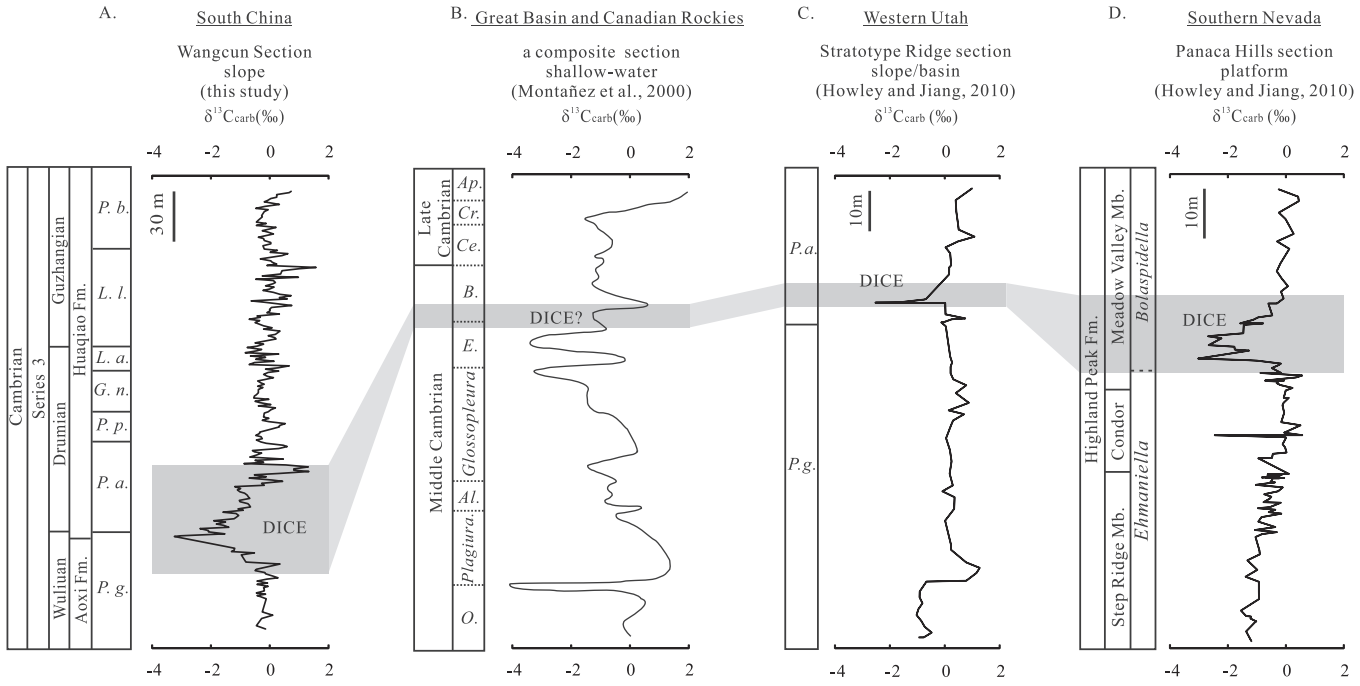

Fig. 4. Correlation of the DICE in various parts of the world. (A) $\delta^{13}C_{carb}$ profile from Wangcun section, South China. (B) composite $\delta^{13}C_{carb}$ curve summarized from shallow-water sections of the Great Basin and Canadian Rockies. Trilobite zones: *Ap.* – *Aphelaspis* Zone; *Cr.* – *Crepicephalus* Zone; *Ce.* – *Cedaria* Zone; *B.* – *Bolaspidella* Zone; *E.* – *Ehmeniella* Zone; *Al.* – *Albertella* Zone; *O.* – *Olenellus* Zone. (C) $\delta^{13}C_{carb}$ profile from Stratotype Ridge section, Western Utah. (D) $\delta^{13}C_{carb}$ profile from Panaca Hills section, Southern Nevada. Fm. – Formation. Mb. – member.

and ten sections in the southern Canadian Rockies (Montañez et al., 2000), the Stratotype Ridge section in western Utah (Howley and Jiang, 2010), and the Panaca Hills section in southern Nevada (Howley and Jiang, 2010). The correlation presented in Fig. 4 is facilitated by well-defined biostratigraphy as illustrated by the key fossils especially *P. atavus* or correlated fauna zone (e.g., *Bolaspidella* Zone). The global $\delta^{13}C_{carb}$ data show that there is a remarkable negative excursion (i.e., the DICE) close to the FAD of *P. atavus* in the slope/basinal sections and nearly coincident with the *Ehmaniella–Bolaspidella* boundary in the shallow-water sections (Fig. 4). The DICE generally begins with $\delta^{13}C_{carb}$ values of approximately 0‰, which decrease to as low as −3.6‰ (Pagès and Schmid, 2016) before returning to pre-excursion values around 0‰ (Fig. 4). Therefore, the DICE documented in the Wangcun section can be well correlated with other sedimentary basins (Fig. 4).

It is worth noting that global correlation of the DICE remains uncertain at a detailed level. It appears as if both the onset and the stratigraphical age of the peak values of the DICE are diachronous and vary between regions (Fig. 4). For example, in the Wangcun section of South China, the onset of the excursion appears to begin below the FAD of *P. atavus*, in the *P. gibbus* Zone (Fig. 4A). In the Stratotype Ridge section in the Drum Mountains which is the type section of the Drumian GSSP, the onset of the DICE seems to begin slightly superjacent to the FAD of *P. atavus*, in the *P. atavus* Zone (Fig. 4C). Moreover, the peak values are different between these basins. The $\delta^{13}C_{carb}$ values of DICE at Wangcun from South China decreased sharply to the minimum value of −3.3‰ just below the base of the Drumian Stage (Fig. 4A), but the DICE from the House Range section in western Utah shows a ~2‰ negative $\delta^{13}C_{carb}$ excursion slightly above the FAD of *P. atavus* (Howley and Jiang, 2010). However, the discrepancies in timing of the onset of the DICE compared to the FAD of the agnostoid trilobite *P. atavus* and in the peak values of the negative $\delta^{13}C_{carb}$ excursion can be attributed to uncertainties in biostratigraphy, differences in the depositional environment, and low sampling resolution (e.g., Howley and Jiang, 2010; Pagès and Schmid, 2016). The biostratigraphic constrains on the position of the first appearance of *P. atavus* is not well identified globally (Howley and Jiang, 2010). The correlation of *P. atavus* Zone to shallow-water *Bolaspidella* Zone is also not well constrained because of poor biostratigraphic control in shallow-water sections (Howley and Jiang, 2010). In addition, the stratigraphic thickness of the unit that recorded the DICE in each sedimentary basin differs significantly (Fig. 4). For example, the DICE covers about 80 m in South China (Fig. 4A), compared to about 7 m in the Stratotype Ridge section of the Drum Mountains, western Utah (Fig. 4C). The excursion of DICE could easily be missed in condensed sections, especially for stratigraphic studies that sampling resolution are relatively low (e.g. > 10 m). In any case, these problems can be resolved by more detailed and high-resolution biostratigrphic and carbon isotopic studies in the future. Therefore, we propose that although there are small differences on a global scale of the DICE excursion compared to the FAD of *P. atavus* (Fig. 4), the consistent negative $\delta^{13}C$ anomaly (i.e. DICE) simultaneously recorded in platform-to-basin sections from different continents favors a profound disturbance to the global carbon cycle rather than local phenomenon.

5.3. Interpretation of the middle Cambrian DICE event

Large negative $\delta^{13}C$ excursions in the middle Cambrian sedimentary records, such as that reported in this study could have resulted from a number of factors including organic carbon burial, which can be linked to primary productivity or anoxia (Kump and Arthur, 1999). The $\delta^{13}C$ value of seawater dissolved inorganic carbon (DIC) can also decrease when the burial of organic carbon decreases. Based on the mass-balance equation for carbon isotopes from Kump and Arthur (1999), a decrease in the proportion of organic carbon to total carbon burial from ~0.14 before the DICE to virtually zero (0.02) immediately after is required to explain the −3.3‰ shift in the $\delta^{13}C$ value of ocean DIC and precipitated carbonate observed in this study (values for variables are shown in Table 2). However, our results show an increase of TOC during this interval. In addition, no abrupt decline of primary productivity has been recorded during the DICE. Therefore, the decrease in primary productivity and potential reduction in organic carbon burial may not have been the major factor responsible for the negative $\delta^{13}C_{carb}$ excursion of the DICE.

Table 2
All parameters used in box model.

Parameter	Initial values	References and notes
M_{DIC}	$\frac{dM_{DIC}}{dt} = F_{in} - F_{out}$	The amount of DIC in the ocean. Modern value: 4×10^{18} mol (Gill et al., 2011).
F_{in}	$F_{in} = F_w + F_{odoc}$	Total input flux of carbon.
F_{out}	$F_{out} = F_{carb} + F_{org}$	Total output flux of carbon ($F_{in} = F_{out}$ at steady state).
F_w	25×10^{18} mol/Ma	Weathering flux (Gill et al., 2011).
F_{org}	$F_{org} = f_{org} \times F_{out}$	Sedimentary output from the oceanic carbon reservoir occurs as burial of organic carbon (F_{org}).
F_{carb}	$F_{carb} = (1 - f_{org}) \times F_{out}$	Sedimentary output from the oceanic carbon reservoir occurs as burial of calcium carbonate (F_{carb}).
f_{org}	0.14	Fraction of carbon buried as organic matter. Value of 0.14 gives $\delta^{13}C$ of DIC of ~0‰ at steady state, similar to values observed at the start of the excursion.
$\delta^{13}C_w$	−4‰	The average carbon isotopic composition of the weathering input (Gill et al., 2011).
$\Delta^{13}C$	29–31‰	Steady-state fractionation during the middle Cambrian (This study).
$\delta^{13}C_{odoc}$	−30‰	A typical value of marine organic carbon during the middle Cambrian (This study).
Sea water volume	1.5×10^9 km^3	Wallmann (2001).
$M_{sulfate}$	2–12 mM or lower	Gill et al. (2011); Loyd et al. (2012).
M_{O2}	3.66×10^{18}–36.6×10^{18} mol	Oxygen content of the atmosphere-ocean system during the DICE (Chameides and Perdue, 1997; Berner, 2006).
K_1	0.87 (36.6×10^{18} mol, 2 mM); 0.52 (36.6×10^{18} mol, 12 mM); 0.39 (3.66×10^{18} mol, 2 mM); 0.10 (3.66×10^{18} mol, 12 mM).	Fraction of organic carbon remineralized by oxygen. Oxygen content (mol) and sulfate concentration (mM) used in our model are shown in parenthesis.
K_2	0.13 (36.6×10^{18} mol, 2 mM); 0.48 (36.6×10^{18} mol, 12 mM); 0.61 (3.66×10^{18} mol, 2 mM); 0.90 (3.66×10^{18} mol, 12 mM).	Fraction of organic carbon remineralized by sulfate. Oxygen content (mol) and sulfate concentration (mM) used in our model are shown in parenthesis.

The negative shifts in both $\delta^{13}C_{carb}$ and $\delta^{13}C_{org}$ can be attributed to the extensive input of isotopically light carbon into the ocean-atmosphere system. Although the exact source of this light carbon into the DICE ocean remains debated, various potential mechanisms have been invoked, including increased ^{12}C-enriched carbon emission during the emplacement of LIP (e.g., Wignall, 2001; Álvaro et al., 2008; Jourdan et al., 2014), increased fresh-water input as uplift and exposure of the platform (Howley and Jiang, 2010; Pagès and Schmid, 2016), and shoaling of ^{12}C-enriched anoxic water associated with a transgressive event (e.g., Howley and Jiang, 2010; Pagès and Schmid, 2016).

The Kalkarindji LIP, which erupted near the early–middle Cambrian boundary (Stage 4–Wuliuan boundary, 510.7 ± 0.6 Ma), has been suggested as a trigger for a series of mass extinctions and negative $\delta^{13}C$ excursions near the Stage 4–Wuliuan boundary (Glass and Phillips, 2006; Álvaro et al., 2008; Jourdan et al., 2014). However, the DICE is coincident with the Wuliuan–Drumian boundary (~506.5 Ma), which is a few million years later (Peng et al., 2012; Jourdan et al., 2014). Furthermore, the emplacement for the main magma volume of LIPs is relatively rapid, ~1 to 3 million years (Bryan and Ernst, 2008, Jourdan et al., 2014). Thus, while LIP events can explain the negative $\delta^{13}C_{carb}$ excursions, it is inconsistent with the accurate timing of DICE. Future accurate geochronology to determine the duration of the Kalkarindji LIP can be used to further explore the relationship between this LIP and the DICE event.

The DICE in both the Great Basin and Georgina Basin is closely associated with the initiation of carbonate platform uplift (Howley and Jiang, 2010; Pagès and Schmid, 2016). Exposure of the platform may have led to increased terrestrial organic matter input as the carbonate platform is exposed to freshwater, resulting in the lower $\delta^{13}C_{carb}$ values in shelf environments (Howley and jiang, 2010; Pagès and Schmid, 2016). This phenomenon has been found in modern and several ancient platform settings (Patterson and Walter, 1994; Immenhauser et al., 2003; Panchuk et al., 2006). However, the Cambrian terrestrial settings would have contributed little organic matter as land plants had not evolved yet. Furthermore, the Wangcun section, which was deposited in a slope-apron environment, was not immediately adjacent to a source of fresh-water that could have supplied low $\delta^{13}C$ carbon (Fig. 1). Thus, fresh-water input is unlikely to be responsible for providing ^{12}C-enriched carbon for the DICE reported globally.

The DICE in worldwide sections appears to universally coincide with a rapid eustatic rising event (Babcock et al. 2007; Ahlberg et al., 2009; Peng et al., 2009; Elfar et al., 2017), suggesting a possible link between the negative $\delta^{13}C_{carb}$ and $\delta^{13}C_{org}$ excursions and a transgressive event. Several lines of evidence suggest sporadic and widespread anoxia of subsurface water masses during the middle Cambrian (Hough et al., 2006; Guo et al., 2010; Pagès and Schmid, 2016; Pagès et al., 2016). Under conditions of deep water anoxia, sea-level rise is often accompanied by strengthened upwelling and widespread shoaling of anoxic deep waters (e.g. Zhuravlev and Wood, 1996; Guo et al., 2010; Gill et al., 2011; Bowyer et al., 2017; Wood et al., 2018). As such, the globally rapid marine transgression during the DICE could have led to incursion of deep anoxic waters into oxygenated shallow water areas. Shoaling of deep anoxic water, which is rich in ^{12}C-enriched DOC, into oxygenated shallow water environment could have led to production of ^{12}C-enriched DIC in the surface water, resulting in the coupled negative $\delta^{13}C_{carb}$ and $\delta^{13}C_{org}$ excursions. The DICE from the Wangcun section is consistent with this model which involves the shoaling of DOC-rich, anoxic deep waters associated with a transgressive event.

5.4. Modelling the DICE excursion and the oxidant budget of the middle Cambrian ocean and atmosphere

As the DICE event represents a major disturbance to the global carbon cycle, we could test the above hypothesis by modelling the ocean inventories of carbon during the DICE. We generated a simple box model (Fig. 5) to explore whether shoaling of anoxic water associated with the transgressive event, accompanied by enhanced oxidative decay of DOC, is capable of reproducing the $\delta^{13}C_{carb}$ and $\delta^{13}C_{org}$ profiles captured in rocks during the DICE. The large oscillations in C-isotopic composition of oceanic DIC reservoir can be associated with a balance of carbon inputs including weathering and oxidative decay of shoaling DOC and carbon outputs including burial of carbonate and organic carbon (Fig. 5). Thus, temporal changes in the C-isotopic composition of the oceanic DIC reservoir (Fig. 5, box 1), as captured by the C-isotopic composition of carbonate minerals that precipitate from seawater, can be expressed as (modified from Kump and Arthur, 1999):

$$\frac{d(\delta^{13}C_{carb})}{dt} = \frac{\delta^{13}C_w \cdot F_w + \delta^{13}C_{odoc} \cdot F_{odoc} - \delta^{13}C_{carb} \cdot F_{carb} - (\delta^{13}C_{carb} - \Delta^{13}C) \cdot F_{org}}{M_{DIC}} \quad (1)$$

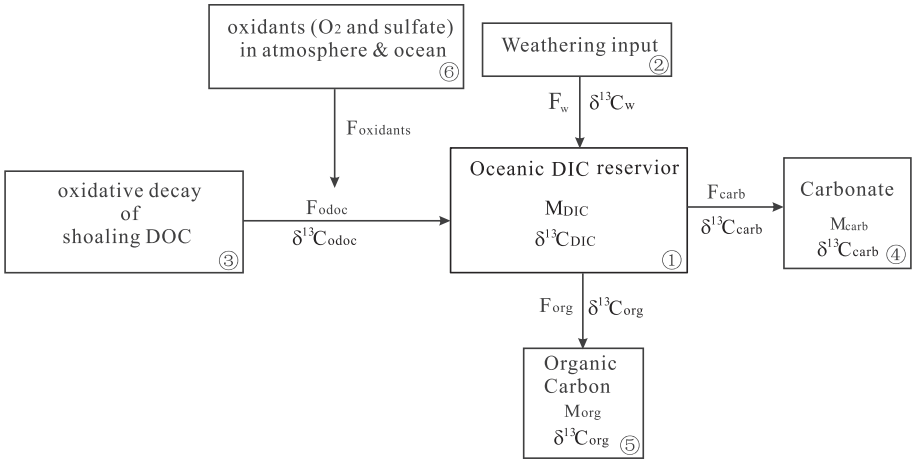

Fig. 5. Isotopic reservoirs and fluxes in the carbon-cycle box model.

where M_{DIC} represents the mass of seawater DIC. F_w refers to the input flux due to weathering (Fig. 5, box 2), while F_{odoc} is the flux of carbon via oxidative decay of shoaling DOC sourced from anoxic deep waters (Fig. 5, box 3). F_{carb} and F_{org} are the output fluxes related to burial of carbonate (Fig. 5, box 4) and organic carbon (Fig. 5, box 5), respectively. $\delta^{13}C_w$ refers to the C-isotopic composition of weathering input, while $\delta^{13}C_{odoc}$ is the C-isotopic composition of the input flux from oxidative decay of shoaling DOC.

And,

$$\delta^{13}C_{org} = \delta^{13}C_{carb} - \Delta^{13}C \quad (2)$$

Then, substituting Eq. (2) into Eq. (1), we arrive at the simplified time-dependent equation for $\delta^{13}C_{org}$:

$$\frac{d(\delta^{13}C_{org})}{dt} = \frac{\delta^{13}C_w \cdot F_w + \delta^{13}C_{odoc} \cdot F_{odoc} - (\delta^{13}C_{org} + \Delta^{13}C) \cdot F_{carb} - \delta^{13}C_{org} \cdot F_{org}}{M_{DIC}} \quad (3)$$

Our simulations are focused on changes in the flux of carbon from oxidative decay of shoaling DOC (F_{odoc}). Oxidative decay of shoaling DOC could introduce an additional flux of ^{12}C-enriched DIC, thus lowering the carbon isotopic composition of the ocean. Importantly, our model puts quantitative constraints on the flux of carbon from oxidative decay of shoaling DOC during the DICE. Fig. 6 shows the sensitivity tests based on transient changes in F_{odoc}, with all other model parameters held constant. The size of F_{odoc} has a large influence on the magnitude of the C-isotope excursion captured by $\delta^{13}C_{carb}$ and $\delta^{13}C_{org}$ (Fig. 6A & B). Increasing F_{odoc} increases the magnitude of the excursions (Fig. 6). Our results show that oxidative decay of 2.1×10^{18} mol/Ma to 4.6×10^{18} mol/Ma of shoaling DOC is necessary to simulate a negative $\delta^{13}C$ excursion of ~2‰ to 4‰ which represent the maximum range of all published DICE excursions (Fig. 4; Fig. 6).

Another important result from the model is that the predicted change in the oxidant budget of the middle Cambrian atmosphere and ocean. The oxidative decay of shoaling DOC is mainly driven by the consumption of oxygen and sulfate from the atmosphere and ocean (Bristow and Kennedy, 2008). Because the DICE-associated transgressive event is recorded in middle Cambrian strata worldwide, the oxidative decay of shoaling DOC would have had significant consequences for the global oxidant inventory of the middle Cambrian ocean-atmosphere system. Assuming the decay of 1 mol of organic carbon to form DOC consumes 1 mol of O_2, and each mole of remineralized organic carbon is oxidized to DIC by 15/8 mol of sulfate (Berner, 2006), the rate of change in the oxidants (O_2 and sulfate) of the middle Cambrian atmosphere and ocean is:

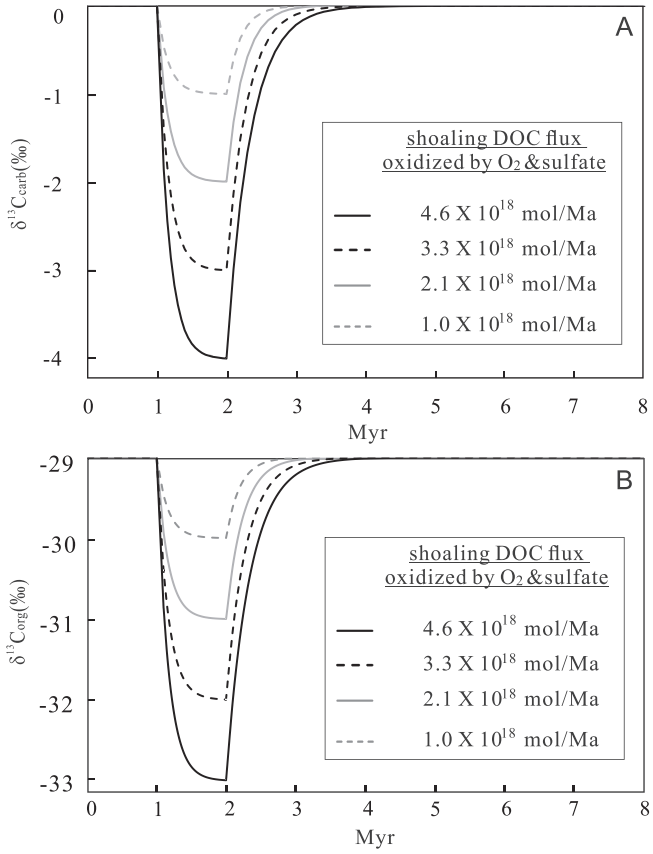

Fig. 6. Modelled $\delta^{13}C_{carb}$ (A) and $\delta^{13}C_{org}$ (B) response to enhanced oxidative decay of shoaling DOC.

$$\frac{d(\text{oxidants})}{dt} = \frac{d(M_{O2} + M_{sulfate})}{dt} = -k_1 \cdot F_{odoc} + \left(-k_2 \cdot \frac{8}{15} \cdot F_{odoc}\right)$$

where M_{O2} and $M_{sulfate}$ represent the oxygen level and sulfate size in the ocean-atmosphere system (Fig. 5, box 6). Constants k_1 and k_2 ($k_2 = 1 - k_1$) represent the fraction of organic carbon remineralized by oxygen and sulfate, respectively, and they are determined by the initial size of oxygen and sulfate reservoirs, such that the consumption of oxidants are at the same relative rate (Bristow and Kennedy, 2008). All initial parameters are shown in Table 2. According to the GEOCARBS-ULF curve (Berner, 2006), the modern value (36.6×10^{18} mol) is proposed as a maximum estimate for the middle Cambrian oxygen level (Berner, 2006; Chen et al., 2015). A minimum oxygen level is set to be

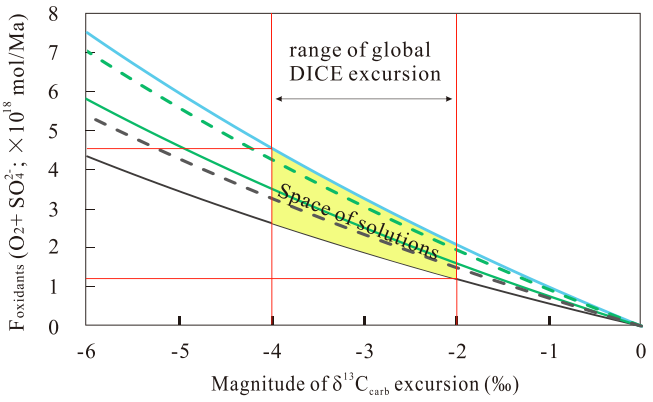

Fig. 7. Oxidants consumption flux ($F_{oxidants}$) versus the magnitude of the $\delta^{13}C_{carb}$ excursion, using oxidant inventories equivalent to modern oxygen content of the atmosphere-ocean system and oceanic sulfate reservoir of 2 mM (green dash curve), modern oxygen content and oceanic sulfate reservoir of 12 mM (green solid curve), 10% modern oxygen content and oceanic sulfate reservoir of 2 mM (black dash curve), 10% modern oxygen content and oceanic sulfate reservoir of 12 mM (black solid curve). The blue solid curve shows the situation if shoaling DOC was totally oxidized by oxygen. The space of solutions that fit our model are highlighted by yellow area. (For interpretation of the references to colour in this figure legend, the reader is referred to the web version of this article.)

10% modern oxygen level, required by the Cambrian biota (Levin, 2003; Sperling et al., 2015). Based on the sulfur isotope and fluid inclusions records, marine sulfate concentration in the middle Cambrian is estimated to be 2–12 mM or lower (e.g., Hough et al., 2006; Gill et al., 2011; Loyd et al., 2012).

We explored the space of solutions of our model using constrains available for seawater sulfate concentration of 2–12 mM or lower, oxygen level of 3.66×10^{18}–36.6×10^{18} mol, and range of global DICE excursion of 2–4‰ (Fig. 7). We have estimated the maximum range of oxidants consumed by shoaling DOC (Fig. 7). As previous studies have argued that the concentration of seawater sulfate in the Cambrian ocean could be very low (< 2 mM) (Hough et al., 2006; Gill et al., 2011; Loyd et al., 2012), the situation that shoaling DOC was totally oxidized by oxygen was considered to be the limiting case in our model (Fig. 7). To generate a ~2‰ to 4‰ negative $\delta^{13}C$ excursion, 1.2×10^{18}–4.6×10^{18} mol/Ma oxidants must have been consumed (Fig. 7). To express these numbers as a net total consumption of oxidants, we need tight temporal constrains. Based on integrated age dates (Peng et al., 2012) and assuming a constant sedimentation rate for the Wangcun section, the duration of falling limb of the DICE leading up to the negative excursion is estimated to be ~1 Ma. Then the oxidative decay of shoaling DOC observed in this study would consume 1.2×10^{18}–4.6×10^{18} mol oxidants during the DICE. These values correspond to 3.0–49.1% decrease in original oxidants in the middle Cambrian atmosphere and ocean.

Our modeling work provides a quantitative framework for understanding the relationship between oxidative decay of shoaling DOC, the size of O_2 and sulfate in atmosphere and ocean, and the $\delta^{13}C$ excursion during the middle Cambrian. Note that, due to a lack of precise radiometric age dating for the middle Cambrian interval and a high degree of freedom in key assumptions in our model, the results from our model are non-unique. However, the modeling results represent the plausible circumstances under which the observed C-isotope excursions could be generated based on sensitivity tests and observations from the geologic record. More importantly, our modeling results provide evidence that enhanced oxidative decay of shoaling DOC may have been linked to a carbon isotope excursion of the magnitude and duration of the DICE.

5.5. Widespread shoaling of DOC-rich, anoxic water and delayed recovery of metazoan reef systems from the early–middle Cambrian mass extinctions

Shoaling of anoxic water has been hypothesized as a trigger to the negative $\delta^{13}C$ excursions (Howley and Jiang, 2010; Zhuravlev and Wood, 1996), and it had a crucial impact on metazoan evolution (Zhuravlev and Wood, 1996). The DICE near the base of Cambrian Drumian Stage were reported in regions worldwide (Fig. 4), indicating a global biogeochemical cycle perturbation. In addition, the DICE appears to be globally concurrent with transgressive event (Babcock et al. 2007; Ahlberg et al., 2009; Peng et al., 2009; Elfar et al., 2017). Therefore, the DICE is thought to have been caused by widespread shoaling of DOC-rich, anoxic water as discussed in this study. The enhanced oxidative decay of shoaling DOC could have provided the isotopic light carbon and resulted in the sudden decrease of $\delta^{13}C$ values. Based on our modeling results, oxidative decay of shoaling DOC during the DICE would have required massive amounts of oxidants, possibly resulting in extensive expansion of anoxia in shallow water environments.

The decline of $\Delta^{13}C$ at the top of the Aoxi Formation provides further evidence for the expansion of anoxic conditions in shallow waters during the DICE. Anoxygenic phototrophs such as green sulfur bacteria use the reductive tricarboxylic acid (TCA) cycle for autotrophic carbon fixation, which produce a smaller carbon isotope fractionation than oxygenic photoautotrophs, such as algae and cyanobacteria which use Calvin cycle (e.g., Quandt et al., 1977; Sirevåg et al., 1977; Summons and Powell, 1986; van Breugel et al., 2005). The increase of green sulfur bacteria biomass to sedimentary organic matter would therefore decrease $\Delta^{13}C$ (Riccardi et al., 2007; Takahashi et al., 2010). Indeed, the report of green sulfur bacteria *Chlorobiaceae*-derived biomarker such as isorenieratane provide strong evidence for pulses of photic zone euxinia associated with the DICE in the Georgina Basin (Pagès and Schmid, 2016). The sharp decrease of $\Delta^{13}C$ corresponded to the DICE in the Wangcun section is consistent with this scenario and suggests widespread and episodic photic zone euxinia during the DICE. We hypothesize that shoaling of anoxic/euxinic waters into shallow waters and the following consumption of oxidants as modeled in this study could play an important role in hindering the recovery of metazoan reef systems from the early–middle Cambrian mass extinctions.

6. Conclusions

The middle Cambrian (Cambrian Series 3) Wuliuan–Drumian boundary interval in the Wangcun section of South China preserves a relatively expanded negative $\delta^{13}C_{carb}$ excursion. This excursion is identified as the DICE, a globally observed negative $\delta^{13}C_{carb}$ excursion that was previously not well recognized in South China. The $\delta^{13}C$ data from the Wangcun section also reveals a negative $\delta^{13}C_{org}$ excursion at approximately the same time as the $\delta^{13}C_{carb}$ excursion (Fig. 2). We interpret the coupled negative $\delta^{13}C_{carb}$ and $\delta^{13}C_{org}$ excursions to reflect the shoaling of ^{12}C-enriched anoxic/euxinic deeper waters associated with a marine transgression. Based on numerical calculations, a carbon isotope excursion of the magnitude and duration of the DICE (2–4‰ decrease over ~1 Ma) would require about 2.1×10^{18} mol/Ma to 4.6×10^{18} mol/Ma of shoaling DOC to be remineralized by oxidants (e.g., O_2 and sulfate) (Fig. 6). Oxidative decay of such large amounts of DOC may have resulted in a transient decrease of oxidants (Fig. 7), causing further expansion of anoxia in shallow waters, thus hindering the recovery of metazoan reef systems from the early–middle Cambrian mass extinctions. Our high-resolution paired $\delta^{13}C_{carb}$ and $\delta^{13}C_{org}$ curves shed new light on global correlations of the DICE to the South China and the paleo-environmental reconstruction of middle Cambrian ocean. Continued exploration of the causes, timing, and magnitude of the DICE from worldwide sections will provide further insight into the chemical conditions of Cambrian oceans.

Acknowledgments

This study was supported by National Natural Science Foundation of China (grants 41890842, 41721002, 41520104007, 41807315, 41673003, 41625013), National Basic Research Program of China (grant 2013CB835003), the 111 project (grant B14026), Chinese Academy of Sciences (grant QYZDY-SSW-DQC031), the Fundamental Research Funds for the Central Universities, and State Key Laboratory of Palaeobiology and Stratigraphy (grant 20191101).

References

Adachi, N., Ezaki, Y., Liu, J., 2014. The late early Cambrian microbial reefs immediately after the demise of archaeocyathan reefs, Hunan Province, South China. Palaeogeogr. Palaeoclimatol. Palaeoecol. 407, 45–55.

Ahlberg, P., Axheimer, N., Babcock, L.E., Eriksson, M.E., Schmitz, B., Terfelt, F., 2009. Cambrian high-resolution biostratigraphy and carbon isotope chemostratigraphy in Scania, Sweden: first record of the SPICE and DICE excursions in Scandinavia. Lethaia 42, 2–16.

Allan, J.R., Matthews, R.K., 1982. Isotope signatures associated with early meteoric diagenesis. Sedimentology 29, 797–817.

Álvaro, J.J., Bauluz, B., Subías, I., Pierre, C., Vizcaïno, D., 2008. Carbon chemostratigraphy of the Cambrian-Ordovician transition in a midlatitude mixed platform, Montagne Noire, France. Geol. Soc. Am. Bull. 120, 962–975.

Babcock, L.E., Robison, R.A., Rees, M.N., Peng, S., Saltzman, M.R., 2007. The global boundary stratotype section and point of the Drumian Stage (Cambrian) in the Drum Mountains, Utah, USA. Episodes 30, 85–95.

Banner, J.L., Hanson, G.N., 1990. Calculation of simultaneous isotopic and trace element variations during water-rock interaction with applications to carbonate diagenesis. Geochim. Cosmochim. Acta 54, 3123–3137.

Berner, R.A., 2006. GEOCARBSULF: a combined model for phanerozoic atmospheric O_2 and CO_2. Geochim. Cosmochim. Acta 70, 5653–5664.

Boucot, A., 1990. Phanerozoic extinctions: how similar are they to each other? In: Kauffman, E.G., Walliser, O.H. (Eds.), Extinction Events in Earth History. Springer, Berlin, pp. 5–30.

Bowyer, F.T., Wood, R.A., Poulton, S.W., 2017. Controls on the evolution of Ediacaran metazoan ecosystems: a redox perspective. Geobiology 15, 516–551.

Bristow, T.F., Kennedy, M.J., 2008. Carbon isotope excursions and the oxidant budget of the Ediacaran atmosphere and ocean. Geology 36, 863–866.

Bryan, S.E., Ernst, R.E., 2008. Revised definition of Large Igneous Provinces (LIPs). Earth-Sci. Rev. 86, 175–202.

Chameides, W.L., Perdue, E.M., 1997. Biogeochemical cycles: a computer-interactive study of Earth system science and global change. Oxford University Press, New York, pp. 224.

Chen, X., Ling, H., Vance, D., Shields-Zhou, G.A., Zhu, M., Poulton, S.W., Och, L.M., Jiang, S., Li, D., Cremonese, L., Archer, C., 2015. Rise to modern levels of ocean oxygenation coincided with the Cambrian radiation of animals. Nat. Commun. 6, 7142.

Derry, L.A., 2010. A burial diagenesis origin for the Ediacaran Shuram-Wonoka carbon isotope anomaly. Earth Planet. Sci. Lett. 294, 152–162.

Derry, L.A., Brasier, M.D., Corfield, R.M., Rozanov, A.Y., Zhuravlev, A.Y., 1994. Sr and C isotopes in Lower Cambrian carbonates from the Siberian craton: a paleoenvironmental record during the 'Cambrian explosion'. Earth Planet. Sci. Lett. 128, 671–681.

Elfar, E.I., Ellwood, B.B., Wang, W.H., Bell, G.L., 2017. Sea level and climatic-induced facies variations in the Middle Cambrian House Range Embayment, western Laurentia. Palaeogeogr. Palaeoclimatol. Palaeoecol. 475, 125–139.

Faggetter, L.E., Wignall, P.B., Pruss, S.B., Sun, Y., Raine, R.J., Newton, R.J., Widdowson, M., Joachimski, M.M., Smith, P.M., 2016. Sequence stratigraphy, chemostratigraphy and facies analysis of Cambrian Series 2–Series 3 boundary strata in northwestern Scotland. Geol. Mag. 155, 865–877.

Gao, G., Land, L.S., 1991. Geochemistry of Cambro-Ordovician Arbuckle limestone, Oklahoma: implications for diagenetic $\delta^{18}O$ alteration and secular $\delta^{13}C$ and $^{87}Sr/^{86}Sr$ variation. Geochim. Cosmochim. Acta 55 (2911–2917), 2919–2920.

Gill, B.C., Lyons, T.W., Young, S.A., Kump, L.R., Knoll, A.H., Saltzman, M.R., 2011. Geochemical evidence for widespread euxinia in the Later Cambrian ocean. Nature 469, 80–83.

Glass, L.M., Phillips, D., 2006. The Kalkarindji continental flood basalt province: a new Cambrian large igneous province in Australia with possible links to faunal extinctions. Geology 34, 461–464.

Guo, Q., Strauss, H., Liu, C., Zhao, Y., Yang, X., Peng, J., Yang, H., 2010. A negative carbon isotope excursion defines the boundary from Cambrian Series 2 to Cambrian Series 3 on the Yangtze Platform, South China. Palaeogeogr. Palaeoclimatol. Palaeoecol. 285, 143–151.

Hayes, J.M., Kaplan, I.R., Wedeking, K.W., 1983. Precambrian organic geochemistry, preservation of the record. In: Schopf, J.W. (Ed.), The Earth's Earliest Biosphere: Its Origin and Evolution. Princeton University Press, Princeton, N.J., pp. 93–134.

Hough, M.L., Shields, G.A., Evins, L.Z., Strauss, H., Henderson, R.A., Mackenzie, S., 2006. A major sulphur isotope event at *c.* 510 Ma: a possible anoxia-extinction-volcanism connection during the Early-Middle Cambrian transition? Terra Nova 18, 257–263.

Howley, R.A., Jiang, G., 2010. The Cambrian Drumian carbon isotope excursion (DICE) in the Great Basin, western United States. Palaeogeogr. Palaeoclimatol. Palaeoecol. 296, 138–150.

Immenhauser, A., Della Porta, G., Kenter, J.A.M., Bahamonde, J.R., 2003. An alternative model for positive shifts in shallow-marine carbonate $\delta^{13}C$ and $\delta^{18}O$. Sedimentology 50, 953–959.

Irwin, H., Curtis, C., Coleman, M., 1977. Isotopic evidence for source of diagenetic carbonates formed during burial of organic-rich sediments. Nature 269, 209–213.

Ishikawa, T., Ueno, Y., Shu, D., Li, Y., Han, J., Guo, J., Yoshida, N., Maruyama, S., Komiya, T., 2014. The $\delta^{13}C$ excursions spanning the Cambrian explosion to the Canglangpuian mass extinction in the Three Gorges area, South China. Gondwana Res. 25, 1045–1056.

Jourdan, F., Hodges, K., Sell, B., Schaltegger, U., Wingate, M.T.D., Evins, L.Z., Söderlund, U., Haines, P.W., Phillips, D., Blenkinsop, T., 2014. High-precision dating of the Kalkarindji large igneous province, Australia, and synchrony with the Early-Middle Cambrian (stage 4–5) extinction. Geology 42, 543–546.

Kaufman, A.J., Knoll, A.H., 1995. Neoproterozoic variations in the C-isotopic composition of seawater: stratigraphic and biogeochemical implications. Precambrian Res. 73, 27–49.

Kump, L.R., Arthur, M.A., 1999. Interpreting carbon-isotope excursions: carbonates and organic matter. Chem. Geol. 161, 181–198.

Lehnert, O., Ahlberg, P., Calner, M., Joachimski, M.M., 2013. The Drumian Isotopic Carbon Excursion (DICE) in Scania, southern Sweden – a mirror of the onset of the Marjumiid Biomere at a time of increased primary production? In: Lindskog, A., Mehlqvist, K. (Eds.), Proceedings of the 3rd IGCP 591 Annual Meeting – Lund, Sweden, 9–19 June 2013. Lund University, pp. 172–174.

Levin, L.A., 2003. Oxygen Minimum Zone benthos: adaptation and community response to hypoxia. Oceanogr. Mar. Biol. Annu. Rev. 41, 1–45.

Li, D., Ling, H., Shields-Zhou, G.A., Chen, X., Cremonese, L., Och, L., Thirlwall, M., Manning, C.J., 2013. Carbon and strontium isotope evolution of seawater across the Ediacaran-Cambrian transition: evidence from the Xiaotan section, NE Yunnan, South China. Precambr. Res. 225, 128–147.

Li, D., Zhang, X., Chen, K., Zhang, G., Chen, X., Huang, W., Peng, S., Shen, Y., 2017. High-resolution C-isotope chemostratigraphy of the uppermost Cambrian stage (Stage 10) in South China: implications for defining the base of Stage 10 and palaeoenvironmental change. Geol. Mag. 154, 1232–1243.

Li, G., Steiner, M., Zhu, X., Yang, A., Wang, H., Erdtmann, B.D., 2007. Early Cambrian metazoan fossil record of South China: generic diversity and radiation patterns. Palaeogeogr. Palaeoclimatol. Palaeoecol. 254, 229–249.

Loyd, S.J., Marenco, P.J., Hagadorn, J.W., Lyons, T.W., Kaufman, A.J., Sour-Tovar, F., Corsetti, F.A., 2012. Sustained low marine sulfate concentrations from the Neoproterozoic to the Cambrian: insights from carbonates of northwestern Mexico and eastern California. Earth Planet. Sci. Lett. 339–340, 79–94.

Montañez, I.P., Osleger, D.A., Banner, J.L., Mack, L.E., Musgrove, M., 2000. Evolution of the Sr and C isotope composition of Cambrian oceans. GSA Today 10, 1–7.

Pagès, A., Schmid, S., 2016. Euxinia linked to the Cambrian Drumian carbon isotope excursion (DICE) in Australia: geochemical and chemostratigraphic evidence. Palaeogeogr. Palaeoclimatol. Palaeoecol. 461, 65–76.

Pagès, A., Schmid, S., Edwards, D., Barnes, S., He, N., Grice, K., 2016. A molecular and isotopic study of palaeoenvironmental conditions through the middle Cambrian in the Georgina Basin, central Australia. Earth Planet. Sci. Lett. 447, 21–32.

Palmer, A.R., 1998. Terminal early Cambrian extinction of the Olenellina: documentation from the Pioche Formation, Nevada. J. Paleontol. 72, 650–672.

Panchuk, K.M., Holmden, C.E., Leslie, S.A., 2006. Local controls on carbon cycling in the Ordovician mid-continent region of North America, with implications for carbon isotope secular curves. J. Sediment. Res. 76, 200–211.

Patterson, W.P., Walter, L.M., 1994. Depletion of ^{13}C in seawater ΣCO_2 on modern carbonate platforms: significance for the carbon isotopic record of carbonates. Geology 22, 885–888.

Peng, S., Babcock, L.E., 2001. Cambrian of the Hunan-Guizhou Region, South China. In: Peng, S.C., Babcock, L.E., Zhu, M.Y. (Eds.), Cambrian System of South China. Palaeoworld, 13. Press of University of Science and Technology of, China, Hefei, pp. 3–51.

Peng, S., Babcock, L.E., Cooper, R.A., 2012. The cambrian period. In: Gradstein, F.M. (Ed.), The Geologic Time Scale 2012, Volume 2: Boston. Elsevier, pp. 437–488.

Peng, S., Babcock, L.E., Zuo, J., Lin, H., Zhu, X., Yang, X., Robison, R.A., Qi, Y., Bagnoli, G., Chen, Y., 2009. The Global boundary Stratotype Section and Point (GSSP) of the Guzhangian Stage (Cambrian) in the Wuling Mountains, northwestern Hunan, China. Episodes 32, 41–55.

Peng, S., Robison, R.A., 2000. Agnostoid biostratigraphy across the middle-upper Cambrian boundary in Hunan, China. J. Paleontol. 74, 1–104.

Pu, X., Ye, H., 1991. Cambrian sedimentary facies and palaeogeography framework in southern China. Coll. Pap. Lith. Paleogeogr. 6, 1–16 [In Chinese with English abstract.].

Quandt, L., Gottschalk, G., Ziegler, H., Stichler, W., 1977. Isptope discrimination by photosynthetic bacteria. FEMS Microbiol. Lett. 1, 125–128.

Riccardi, A., Kump, L.R., Arthur, M., D'Hondt, S., 2007. Carbon isotopic evidence for chemocline upward excursions during the end-Permian event. Palaeogeogr. Palaeoclimatol. Palaeoecol. 248, 73–81.

Schidlowski, M., Aharon, P., 1992. Carbon cycle and carbon isotope record: geochemical impact of life over 3.8 Ga of Earth history. In: Schidlowski, M., Golubic, S., Kimberley, M.M., McKirdy, D.M., Trudinger, P.A. (Eds.), Early Organic Evolution: Implications for Mineral and Energy, Resources, pp. 147–175.

Sirevåg, R., Buchanan, B.B., Berry, J.A., Troughton, J.H., 1977. Mechanisms of CO_2 fixation in bacterial photosynthesis studied by the carbon isotope fractionation technique. Arch. Microbiol. 112, 35–38.

Sperling, E.A., Wolock, C., Morgan, A.S., Gill, B.C., Kunzmann, M., Harverson, G.P., Macdonald, F.A., Knoll, A.H., Johnston, D.T., 2015. Statistical analysis of iron geochemical data suggests limited late Proterozoic oxygenation. Nature 523, 451–454.

Summons, R.E., Powell, T.G., 1986. *Chlorobiaceae* in Palaeozoic seas revealed by

biological markers, isotopes and geology. Nature 319, 763–765.
Takahashi, S., Kaiho, K., Oba, M., Kakegawa, T., 2010. A smooth negative shift of organic carbon isotope ratios at an end-Permian mass extinction horizon in central pelagic Panthalassa. Palaeogeogr. Palaeoclimatol. Palaeoecol. 292, 532–539.
van Breugel, Y., Schouten, S., Paetzel, M., Ossebaar, J., Sinninghe Damste, J.S., 2005. Reconstruction of $\delta^{13}C$ of chemocline CO_2 (aq) in past oceans and lakes using the $\delta^{13}C$ of fossil isorenieratene. Earth Planet. Sci. Lett. 235, 421–434.
Wallmann, K., 2001. Controls on the cretaceous and Cenozoic evolution of seawater composition, atmospheric CO_2 and climate. Geochim. Cosmochim. Acta 65, 3005–3025.
Wignall, P.B., 2001. Large igneous provinces and mass extinctions. Earth-Sci. Rev. 53, 1–33.
Wood, R., 1999. In: Reef Evolution. Oxford University Press, Oxford, pp. 414.
Wood, R., Bowyer, F., Penny, A., Poulton, S.W., 2018. Did anoxia terminate Ediacaran benthic communities? Evidence from early diagenesis. Precambr. Res. 313, 134–147.
Zhu, M., Zhang, J., Li, G., Yang, A., 2004. Evolution of C isotopes in the Cambrian of China: implications for Cambrian subdivision and trilobite mass extinctions. Geobios 37, 287–301.
Zhuravlev, A.Y., Wood, R.A., 1996. Anoxia as the cause of the mid-Early Cambrian (Botomian) extinction event. Geology 24, 311–314.